J. Fluid Mech. (1982), *vol.* 121, *pp.* 107–122
Printed in Great Britain

A dynamic runaway effect associated with flux expulsion in magnetohydrodynamic channel flow

By H. KAMKAR†
School of Mathematics, University of Bristol
AND H. K. MOFFATT
Department of Applied Mathematics and Theoretical Physics, Silver Street, Cambridge

(Received 3 October 1981)

Pressure-driven flow along a channel in the presence of an applied magnetic field which is periodic in the streamwise direction is considered. The configuration is such that the transverse component of field B_y is non-zero on the centreline $y = 0$, but its streamwise average $\langle B_y \rangle$ is zero. In this situation, flux expulsion due to reconnection of field lines occurs when the pressure gradient is sufficiently large. This leads to a decrease in the Lorentz forces, hence to an acceleration of the flow, and hence to stronger flux expulsion. When viscous effects are weak (i.e. at high Hartmann number) this creates a runaway effect, which appears at a critical value of the pressure gradient. This critical value is determined in the inviscid limit, and numerical and analytical methods are used to explore the associated 'cusp-catastrophe' behaviour when effects of weak viscosity are taken into account.

1. Introduction

The phenomenon of 'flux expulsion' in magnetohydrodynamics occurs at high magnetic Reynolds number, whenever a flow with closed streamlines acts upon a magnetic field transverse to the flow. The purely kinematic aspects of this phenomenon have been widely studied (Zel'dovich 1957; E. N. Parker 1963; R. L. Parker 1966; Weiss 1966) and are well understood. It is also known (Galloway, Proctor & Weiss 1978; Proctor & Galloway 1979) that flux expulsion can persist even in circumstances in which the magnetic field has a strong dynamic influence.

In this paper, we study an aspect of the dynamic behaviour associated with flux expulsion, which has been investigated in the simpler context of *solid* conducting rotors by Gimblett & Peckover (1979); this is that, as the forces which drive the motion are *increased*, the ohmic resistance to motion can *decrease*, leading to a 'runaway' situation in which the kinetic energy of the motion increases very rapidly, being ultimately controlled by any other weak dissipative processes that may be present. This behaviour was recognized by Gimblett & Peckover as a typical 'cusp-catastrophe' behaviour, with associated hysteresis effects. The same type of behaviour in a fluid context (rotation of a fluid cylinder in the presence of a rotating transverse field) has been identified by Moffatt (1980).

If the flow does not have closed streamlines, flux expulsion can still occur provided

† Present address: Berkeley Nuclear Laboratories, Berkeley, Gloucester, England.

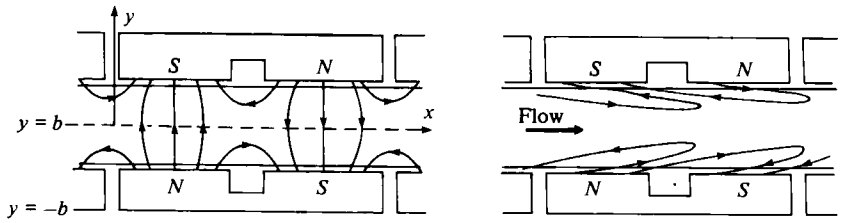

FIGURE 1. Sketch of configuration considered: (*a*) magnetic field with no flow; (*b*) magnetic field showing flux expulsion due to flow under applied pressure gradient.

that the applied field is non-uniform, and a particle trajectory crosses a region or regions in which the transverse component of applied field changes sign. The configuration of figure 1, which we study in this paper, falls within this general category. Specifically we consider the plane two-dimensional flow of an incompressible fluid of density ρ and electrical conductivity σ, along a channel $|y| < b$, driven by an applied pressure gradient $-\rho G$, and in the presence of a magnetic field **B** whose normal component B_y is prescribed† on the boundaries in the form

$$B_y = B_0 \cos kx \quad \text{on} \quad y = \pm b. \tag{1.1}$$

Figure 1 (*a*) shows a distribution of electromagnets which could (in idealized circumstances) produce such a field, and the resulting flux lines when the fluid is at rest (i.e. when $G = 0$). This type of configuration is of potential importance in the context of liquid-metal cooling circuits of breeder reactors; here, magnetic fields may be used to control the flow structure, and it is important to understand the influence of non-uniform fields, among which the field of figure 1 (*a*) may be regarded as a particular prototype.

Consider first, in a qualitative manner, what happens when G increases through positive values. Assuming that the flow is laminar, the field **B** and velocity **u** will be periodic in x with period $2\pi/k$. Let U and B represent average values (with respect to x) of u_x and $|B_y|$ on the centreline $y = 0$. B and U are related through the induction equation and the equation of motion. The induction equation describes the distortion of flux lines in the downstream direction, and the elimination of strong field gradients by ohmic diffusion. When U is large, this process will evidently result in expulsion of flux from the core region of the duct, and the formation of magnetic boundary layers on $y = \pm b$ (figure 1*b*); we may therefore infer a relationship

$$B = F(U), \tag{1.2}$$

where $F(U)$ is monotonic decreasing, and exponentially small as $U \to \infty$. (The fact that the asymptotic decrease is exponential is confirmed by the analysis of §4.2 below.) This is represented by the solid curve of figure 2 (*a*), which may be described as the *flux equilibrium curve*.

† A referee has pointed out that, if the exciting current consists of a current sheet $\mathbf{J}_s \sin kx$ on $y = \pm b$, the regions $|y| > b$ being filled with highly permeable material, then it is B_x rather than B_y that is prescribed on $y = \pm b$. This leads to a rather different boundary-value problem, but with similar qualitative behaviour.

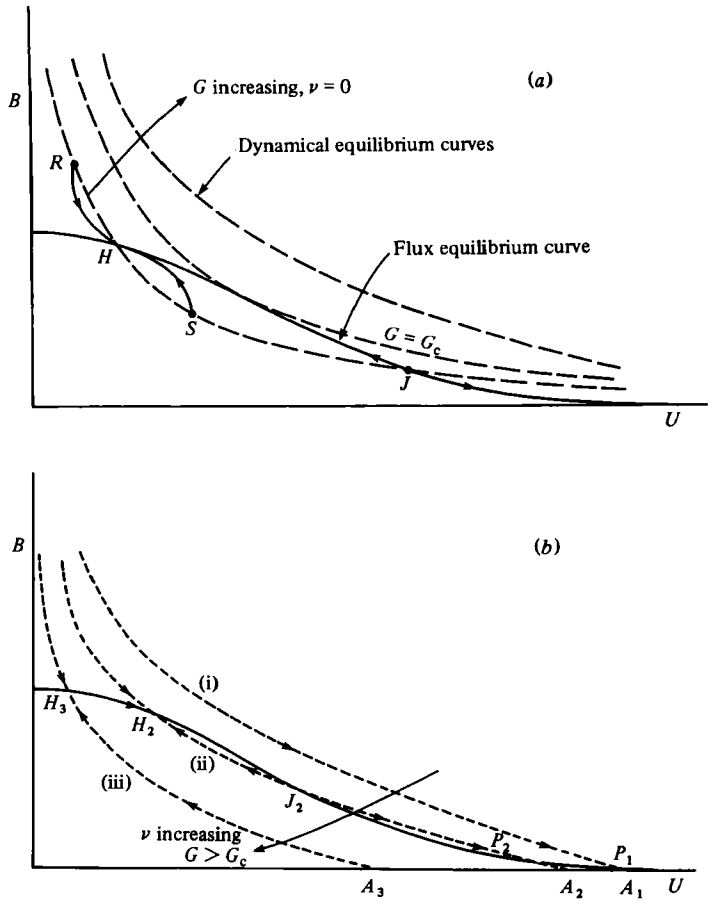

FIGURE 2. Flux equilibrium curve (solid) and dynamic equilibrium curves (dashed). Intersections represent possible steady states which are of Hartmann type (H) or Poiseuille type (P); states labelled J are unstable. (a) Inviscid situation, showing runaway behaviour if $G > G_c$; (b) weakly viscous situation, showing the possibility of three solutions (H_2, J_2, P_2).

Consider now the dominant force balance in the equation of motion. The induced currents in the core are of order

$$j \sim \sigma UB, \tag{1.3}$$

and the Lorentz force is of order

$$F \sim jB \sim \sigma UB^2. \tag{1.4}$$

If viscous forces are negligible, then a steady state is possible only if this force is in equilibrium with the applied pressure gradient, i.e.

$$\sigma UB^2 \sim \rho G. \tag{1.5}$$

This simple relationship between U and B is represented (for different values of G) by the dashed curves of figure 2(a), which may be described as *dynamic equilibrium curves*.

Both the induction equation and the equation of motion can be satisfied only at points of intersection of a dashed curve with the solid curve, e.g. at the points H and

J in figure 2(a). The point H represents a stable equilibrium, whereas the point J represents an unstable equilibrium; this may be seen by considering the behaviour of the system at points such as R or S. Suppose that G is given and that we start at the point R on the corresponding dynamic equilibrium curve. At R, B is greater than is required by flux equilibrium; consequently flux is expelled and B decreases. The Lorentz force then decreases and so the flow accelerates, i.e. U increases. We thus follow a path in the (B, U)-plane from R towards H as indicated in the figure. Similarly if we start at the point S, B increases and U decreases until again we arrive at H. Hence H is stable. Similarly J is unstable.

If G exceeds a critical value G_c for which the dashed curve *touches* the flux equilibrium curve, then there is no intersection and therefore no possibility of an 'inviscid' steady-state solution. We have then a 'runaway' situation: as the flow accelerates under the applied pressure gradient the flux-expulsion effect is so strong that there is a dramatic decrease in the resisting Lorentz force; in this situation the velocity can only be controlled by viscosity (no matter how weak this may be).

The effect of weak viscosity may be crudely represented by modifying the estimate (1.5) to the form

$$\sigma U B^2 + \rho \nu U / b^2 \sim \rho G. \tag{1.6}$$

The dynamic equilibrium curves are then shifted downwards slightly (the dotted curves of figure 2b), each curve intersecting the axis $B = 0$ at the Poiseuille value $U_P \sim Gb^2/\nu$. Three possible curves are shown in figure 2(b) labelled (i), (ii), (iii). Curve (i) is a 'runaway' curve which now intersects the flux equilibrium curve at the point P_1, very near to the Poiseuille value (represented by A_1). Curve (ii) shows three intersections H_2, J_2 and P_2, of which H_2 and P_2 are stable and J_2 is unstable. As ν increases further, we lose the intersections J and P, and (curve (iii)) we have again a single intersection at H_3; this flow is characterized by strong field and weak velocity, and is more akin to Hartmann flow than to Poiseuille flow.

The above description is of course purely qualitative, but the more detailed analysis of the subsequent sections corroborates this description, and provides a quantitative determination of the critical pressure gradient at which runaway occurs.

2. Mean-flow equations

In order to provide this quantitative analysis, we need to replace (1.2) and (1.6) by the appropriate governing differential equations for mean fields (averaged over x), and solve these either analytically or numerically. We shall, for the moment, retain time-dependence in these equations, which can then also describe the approach to equilibrium (as represented for example by the trajectory $R \to H$ in figure 2a).

Let $\mathbf{A} = A(x, y, t)\,\mathbf{i}_z$ be the vector potential of the field $\mathbf{B}$ (satisfying $\nabla . \mathbf{A} = 0$), i.e.

$$B_x = \partial A/\partial y, \quad B_y = -\partial A/\partial x. \tag{2.1}$$

The current distribution in the fluid is then

$$\mathbf{j} = \mu_0^{-1} \nabla \wedge \mathbf{B} = -\mu_0^{-1} \nabla^2 A \mathbf{i}_z, \tag{2.2}$$

and the Lorentz force is

$$\mathbf{F} = \mathbf{j} \wedge \mathbf{B} = -\mu_0^{-1} (\nabla^2 A)\, \nabla A. \tag{2.3}$$

The electric field $\mathbf{E}$ is given by

$$\mathbf{E} = -\mathbf{i}_z \partial A/\partial t - \nabla \phi, \tag{2.4}$$

and is related to $\mathbf{j}$ by Ohm's law,

$$\mathbf{j} = \sigma(\mathbf{E} + \mathbf{u} \wedge \mathbf{B}), \tag{2.5}$$

where $\mathbf{u}(x, y, t)$ is the velocity field, satisfying $\nabla . \mathbf{u} = 0$. Since $\nabla . \mathbf{j} = 0$ and the flow is two-dimensional, the divergence of (2.5) gives

$$\nabla^2 \phi = 0, \tag{2.6}$$

so that the electrostatic contribution $-\nabla\phi$ to $\mathbf{E}$ is determined by the remote boundary conditions. In conventional Hartmann flow, with a *uniform* applied field, this contribution provides the means of closing the current circuit, either within the fluid or within the duct boundary (see e.g. Hunt & Shercliff 1971). In the present context, however, the periodicity in the x-direction implies that the net flux of $\mathbf{j}$ in the z-direction is zero, and the problem of 'closing the current circuit' does not arise. We shall suppose that there is no externally applied electric field, and in particular that there is no externally maintained potential difference between the remote boundaries $z = \pm z_0$ (where $z_0 \gg b$). There will of course be boundary layers on $z = \pm z_0$ which will depend on their electrical properties, but outside these layers the assumption of a two-dimensional flow and field is justified, and the relevant solution of (2.6) is $\phi = \text{cst}$; (2.5) then gives, in the usual way,

$$\partial A/\partial t + \mathbf{u} . \nabla A = \lambda \nabla^2 A, \tag{2.7}$$

where $\lambda = (\mu_0 \sigma)^{-1}$.

The Navier–Stokes equation is

$$\partial \mathbf{u}/\partial t + \mathbf{u} . \nabla \mathbf{u} = -\rho^{-1} \nabla P - (\mu_0 \rho)^{-1} (\nabla^2 A) \nabla A + \nu \nabla^2 \mathbf{u}, \tag{2.8}$$

where

$$\langle \partial P/\partial x \rangle = -\rho G \tag{2.9}$$

is the applied pressure gradient, which we suppose to be constant. Here, and subsequently, the angular brackets $\langle\ \rangle$ denote averaging over a wavelength $2\pi/k$ in the x-direction.

Now let

$$\mathbf{u} = U(y, t)\, \mathbf{i}_x + \mathbf{u}'(x, y, t), \tag{2.10}$$

where

$$\mathbf{u}' = (u', v', 0), \quad \langle \mathbf{u}' \rangle = 0. \tag{2.11}$$

It is obvious from the periodicity of the applied field that

$$\langle A \rangle = 0. \tag{2.12}$$

The average of (2.7) then gives

$$\partial \langle v' A \rangle / \partial y = 0, \quad \text{i.e.} \quad \langle v' A \rangle = f_1(t), \text{ say}, \tag{2.13}$$

and the average of the two components of (2.8) gives

$$\partial U/\partial t + \partial \langle u' v' \rangle / \partial y = G - (\mu_0 \rho)^{-1} \langle \partial A/\partial x \nabla^2 A \rangle + \nu\, \partial^2 U/\partial y^2, \tag{2.14}$$

$$\partial \langle v'^2 \rangle / \partial y = -\rho^{-1} \partial \langle P \rangle / \partial y - (\mu_0 \rho)^{-1} \langle \partial A/\partial y \nabla^2 A \rangle; \tag{2.15}$$

the latter integrates, in conjunction with (2.9), to give

$$\langle v'^2 \rangle + (2\mu_0 \rho)^{-1} \langle (\nabla A)^2 \rangle = Gx + f_2(t). \tag{2.16}$$

The equations for the fluctuating fields A, $\mathbf{u}'$ and $P' = P - \langle P \rangle$ are now simply obtained; the fluctuating part of (2.7) is

$$\frac{\partial A}{\partial t} + U \frac{\partial A}{\partial x} + \underline{\nabla . (\mathbf{u}' A - \langle \mathbf{u}' A \rangle)} = \lambda \nabla^2 A, \tag{2.17}$$

and the fluctuating part of (2.8) is

$$\frac{\partial \mathbf{u}'}{\partial t}+U\frac{\partial \mathbf{u}'}{\partial x}+\underline{\nabla.(\mathbf{u}'\mathbf{u}'-\langle \mathbf{u}'\mathbf{u}'\rangle)}=-\frac{1}{\rho}\nabla P'-\frac{1}{\mu_0\rho}(\nabla^2 A\nabla A-\langle\nabla^2 A\nabla A\rangle)+\nu\nabla^2\mathbf{u}'. \quad (2.18)$$

The underlined terms involve interaction of fluctuating quantities, and the treatment of such terms is in general exceedingly awkward. If, however, conditions are such that

$$|\mathbf{u}'|\ll U, \quad (2.19)$$

then these underlined terms will be negligible compared with $U\partial A/\partial x$ (in (2.17)) and $U\partial \mathbf{u}'/\partial x$ (in (2.18)). Let us suppose that this is the case; then, provided we are not too far from equilibrium, the dominant balance in (2.17) is between mean convection and diffusion, i.e.

$$U\partial A/\partial x\sim\lambda\nabla^2 A \quad (2.20)$$

in order of magnitude (cf. (1.3)), and, assuming viscous effects are weak, the dominant balance in (2.14) is

$$G\sim(\mu_0\rho)^{-1}\langle\partial A/\partial x\,\nabla^2 A\rangle\sim(\mu_0\rho\lambda)^{-1}U\langle B_y^2\rangle \quad (2.21)$$

(cf. (1.4)). Likewise, the dominant balance of the x-component of (2.18) is

$$U\partial u'/\partial x\sim-(\mu_0\rho\lambda)^{-1}U(B_y^2-\langle B_y^2\rangle), \quad (2.22)$$

or, again in order of magnitude,

$$Uk|u'|\sim(\mu_0\rho\lambda)^{-1}U\langle B_y^2\rangle\sim G. \quad (2.23)$$

Hence

$$\frac{|u'|}{U}\sim\frac{G}{kU^2}\sim\frac{\langle B_y^2\rangle^2}{k(\mu_0\rho\lambda)^2 G}. \quad (2.24)$$

Now $\langle B_y^2\rangle\leqslant\frac{1}{2}B_0^2$ (with equality only at the boundaries $y=\pm b$), and so (2.24) becomes

$$\frac{|u'|}{U}\lesssim\frac{B_0^4}{4k(\mu_0\rho\lambda)^2 G}. \quad (2.25)$$

The above argument is self-consistent provided that (2.19) is satisfied, i.e. provided that

$$B_0^4\ll k(\mu_0\rho\lambda)^2 G, \quad (2.26)$$

and we shall suppose that this condition is satisfied in what follows.

It is easily verified that

$$\frac{1}{G}\frac{\partial}{\partial y}\langle u'v'\rangle\sim\frac{B_0^4}{k(\mu_0\rho\lambda)^2 G}, \quad (2.27)$$

so that the Reynolds-stress term in (2.14) is also negligible when (2.26) is satisfied. Hence (2.17) and (2.14) become

$$\partial A/\partial t+U\partial A/\partial x=\lambda\nabla^2 A, \quad (2.28)$$

$$\partial U/\partial t=G-(\mu_0\rho)^{-1}\langle\partial A/\partial x\,\nabla^2 A\rangle+\nu\partial^2 U/\partial y^2, \quad (2.29)$$

and we have to solve these equations subject to the boundary conditions

$$\left.\begin{aligned}\partial A/\partial x&=-B_0\cos kx\\ U&=0\end{aligned}\right\}\quad\text{on}\quad y=\pm b \quad (2.30)$$

and appropriate initial conditions.

Let us now introduce dimensionless variables

$$\eta = y/b, \quad \tau = b^2 kG\lambda^{-1}t, \tag{2.31}$$

and let

$$A = B_0 k^{-1}\mathscr{R}[if(\eta,\tau)\,e^{ikx}], \tag{2.32a}$$

$$U = (\lambda/b^2k)\,\hat{U}. \tag{2.32b}$$

Then (2.28) and (2.29) become

$$\beta\frac{\partial f}{\partial\tau} + i\hat{U}f = \left(\frac{\partial^2}{\partial\eta^2} - \kappa^2\right)f, \tag{2.33a}$$

$$\frac{\partial\hat{U}}{\partial\tau} = 1 - \frac{1}{2Q}\mathscr{R}\left[if\left(\frac{\partial^2}{\partial\eta^2} - \kappa^2\right)f^*\right] + \epsilon\frac{\partial^2\hat{U}}{\partial\eta^2}, \tag{2.33b}$$

where

$$\beta = \frac{b^4kG}{\lambda^2}, \quad Q = \frac{\mu_0\rho b^2kG}{B_0^2}, \quad \kappa = kb, \quad \epsilon = \frac{\nu\lambda}{b^4kG}, \tag{2.34}$$

the four independent dimensionless parameters that characterize the problem. In terms of these parameters, the condition (2.26) becomes simply

$$\beta \ll Q^2. \tag{2.35}$$

Note that the Hartmann number $M = B_0 b/(\mu_0\rho\lambda\nu)^{\frac{1}{2}}$ and the magnetic Prandtl number $P_m = \nu/\lambda$ are related to these parameters by

$$M = (Q\epsilon)^{-\frac{1}{2}}, \quad P_m = \beta\epsilon. \tag{2.36}$$

We shall be particularly concerned with the situation when $\kappa = O(1)$, $Q = O(1)$ and $\epsilon \ll 1$, so that

$$M \gg 1, \quad P_m \ll 1. \tag{2.37}$$

The latter condition is realistic in the context of liquid metals, for which P_m is generally in the range 10^{-5}–10^{-7}.

The boundary conditions associated with (2.33) are (from (2.30))

$$f(\pm 1,\tau) = 1, \quad \hat{U}(\pm 1,\tau) = 0. \tag{2.38}$$

However, it is clear that both f and U are even functions of η; we may therefore restrict attention to the interval $0 < \eta < 1$, and adopt boundary conditions

$$f_\eta = 0, \quad \hat{U}_\eta = 0 \quad \text{on} \quad \eta = 0, \tag{2.39a}$$

$$f = 1, \quad \hat{U} = 0 \quad \text{on} \quad \eta = 1. \tag{2.39b}$$

If $\beta \ll 1$, (2.33*a*, *b*) may be further simplified. In this situation, the adjustment to 'flux equilibrium' is instantaneous, and the term $\beta\,\partial f/\partial\tau$ in (2.33*a*) can be dropped. We then have

$$i\hat{U}f = (\partial^2/\partial\eta^2 - \kappa^2)f, \tag{2.40a}$$

$$\partial\hat{U}/\partial\tau = 1 - (2Q)^{-1}\hat{U}|f|^2 + \epsilon\,\partial^2\hat{U}/\partial\eta^2, \tag{2.40b}$$

equations which, in effect, describe evolution *along* the flux equilibrium curve of figure 2(*a*) or 2(*b*).

In the computational work described in the following sections, the parameter β in (2.33*a*, *b*) was set equal to unity; this must merely be regarded as a computationally convenient choice: any conclusions concerning steady-state solutions of (2.33*a*, *b*) are independent of the value of β chosen, and would be the same if, instead, a small value satisfying (2.35) were chosen.

3. Conditions for the existence of a steady inviscid solution

We may expect, from the introductory discussion, that in the inviscid limit ($\epsilon = 0$) a steady solution of (2.33) and (2.38) will exist† only if Q is not too large, i.e. only for $Q < Q_c(\kappa)$, where $Q_c(\kappa)$ is a function to be determined. The critical 'runaway' pressure gradient (from (2.34b)) will then be given by

$$\rho G_c = \frac{B_0^2}{\mu_0 b}\kappa^{-1}Q_c(\kappa). \tag{3.1}$$

Suppose first that a steady solution $\{f(\eta), \hat{U}(\eta)\}$ does exist. Let

$$f(\eta) = p(\eta)\exp[iq(\eta)], \tag{3.2}$$

where, from (2.38),

$$\left.\begin{aligned} p'(0) = q'(0) = 0, \\ p(1) = 1, \quad q(1) = 0. \end{aligned}\right\} \tag{3.3}$$

Then with ($\epsilon = 0$), the steady form of (2.33) becomes

$$p'' - pq'^2 - \kappa^2 p = 0, \tag{3.4a}$$

$$2p'q' + pq'' = \hat{U}p, \tag{3.4b}$$

$$\hat{U}p^2 = 2Q. \tag{3.4c}$$

Note that, since $p(1) = 1$, and $\hat{U}$ must be finite, we must have

$$p(\eta) > 0 \quad (0 \leqslant \eta \leqslant 1). \tag{3.5}$$

We may now eliminate $\hat{U}$ and q from (3.4) to obtain a single equation for p; for

$$2Q = \hat{U}p^2 = p(2p'q' + pq'') = (p^2q')', \tag{3.6}$$

and so, since $q'(0) = 0$,

$$p^2q' = 2Q\eta. \tag{3.7}$$

Hence (3.4a) becomes

$$p'' = \kappa^2 p + \frac{4Q^2\eta^2}{p^3}, \tag{3.8}$$

and we have the boundary conditions

$$p'(0) = 0, \quad p(1) = 1. \tag{3.9}$$

This defines an intriguing nonlinear two-point boundary-value problem. The solution, if it exists, must evidently satisfy

$$0 < p(\eta) \leqslant 1, \quad p''(\eta) > 0 \quad (0 \leqslant \eta \leqslant 1). \tag{3.10}$$

An alternative statement of the problem involves the Green function $G(\xi, \eta)$ defined by

$$G(\xi, \eta) = \frac{\sinh\kappa(1-\xi)\cosh\kappa\eta}{\kappa\cosh\kappa} \quad (\eta < \xi) \tag{3.11}$$

(and $G(\eta, \xi) = G(\xi, \eta)$). It may easily be shown that $p(\eta)$ satisfies the nonlinear integral equation

$$p(\eta) = \frac{\cosh\kappa\eta}{\cosh\kappa} - 4Q^2\int_0^1 \frac{\xi^2 G(\xi, \eta)}{(p(\xi))^3}\,d\xi. \tag{3.12}$$

† The no-slip condition $\hat{U}(1) = 0$ is of course dropped in the inviscid limit.

We may deduce a *necessary* condition for the existence of a solution; for the condition $p(0) > 0$ implies that

$$4Q^2 \int_0^1 \frac{\xi^2 G(\xi, 0)}{(p(\xi))^3}\, d\xi < \frac{1}{\cosh \kappa}. \tag{3.13}$$

Hence, since $p(\xi) < 1$,

$$4Q^2 \int_0^1 \xi^2 \kappa^{-1} \sinh \kappa(1-\xi)\, d\xi < 1, \tag{3.14}$$

or, evaluating the integral,

$$Q < Q_1(\kappa), \tag{3.15}$$

where

$$Q_1(\kappa) = \frac{\kappa^2}{2^{\frac{3}{2}}(\cosh \kappa - 1 - \frac{1}{2}\kappa^2)^{\frac{1}{2}}} \sim \begin{cases} 3^{\frac{1}{2}}(1 - \frac{1}{60}\kappa^2 - \frac{9}{50\,400}\kappa^4 + \ldots) & \text{as } \kappa \to 0, \\ \frac{1}{2}\kappa^2 e^{-\frac{1}{2}\kappa} & \text{as } \kappa \to \infty. \end{cases} \tag{3.16}$$

A second necessary condition for the existence of a solution,† which is significantly stronger than (3.15) in the range $1{\cdot}1 \lesssim \kappa \lesssim 33$, may be obtained by regarding the right-hand side of (3.8) as a function $f(p)$ which has a minimum at

$$p = p_{\mathrm{m}} = (12Q^2\eta^2/\kappa^2)^{\frac{1}{4}}, \tag{3.17}$$

so that, for $0 \leqslant \eta \leqslant 1$,

$$p'' > f(p_{\mathrm{m}}) = C\eta^{\frac{1}{2}}, \quad \text{where} \quad C = 4\left(\frac{2Q\kappa^3}{3\sqrt{3}}\right)^{\frac{1}{2}}. \tag{3.18}$$

Hence, using $p'(0) = 0$,

$$p(\eta) > p(0) + \tfrac{4}{15}C\eta^{\frac{5}{2}} > \tfrac{4}{15}C\eta^{\frac{5}{2}}, \tag{3.19}$$

and so, since $p(1) = 1$, it follows that $C < \frac{15}{4}$, or equivalently

$$Q < Q_2(\kappa) = \frac{3^{\frac{7}{2}}5^2}{2^9}\kappa^{-3} \approx 2{\cdot}283\,\kappa^{-3}. \tag{3.20}$$

The functions $Q_1(\kappa)$, $Q_2(\kappa)$ are plotted in figure 3; the above argument establishes that, for

$$Q > \min\,(Q_1(\kappa), Q_2(\kappa)), \tag{3.21}$$

the runaway effect definitely does occur.

The exact necessary *and* sufficient condition for the existence of a solution, $Q < Q_{\mathrm{c}}(\kappa)$, can only be determined numerically, either by numerical integration of (3.8) and (3.9), gradually increasing Q from zero for each fixed κ, or by returning to the unsteady equations (2.33*a*, *b*) with $\epsilon = 0$, and integrating step by step in time for different values of κ and Q, to determine the region of the (κ, Q)-plane in which the solution approaches a steady state; obviously this does not depend on the value of β, since the steady-state characteristics do not depend on β. We adopted this latter technique, which was then later easily modified to include viscosity effects ($\epsilon > 0$). Figures 4(*a*, *b*) show the computed development‡ of the velocity profile $\hat{U}(\eta, \tau)$ for $\epsilon = 0$ in two cases:

(*a*) $\kappa = 10^{-4}$, $Q = 0{\cdot}6$, in which $\hat{U}$ evidently approaches a steady state as $\tau \to \infty$; and

(*b*) $\kappa = 3$, $Q = 0{\cdot}005$, in which the centreline velocity accelerates without limit, indicating that we are clearly in the runaway regime.

By increasing Q for each fixed κ, the value $Q_{\mathrm{c}}(\kappa)$, at which the transition occurs from behaviour of type (*a*) to behaviour of type (*b*), was determined. The curve

† We are indebted to Dr M. R. E. Proctor, who suggested the argument of this paragraph.

‡ Full computational details may be found in Kamkar (1981); the value of β actually adopted in these computations was $\beta = 1$.

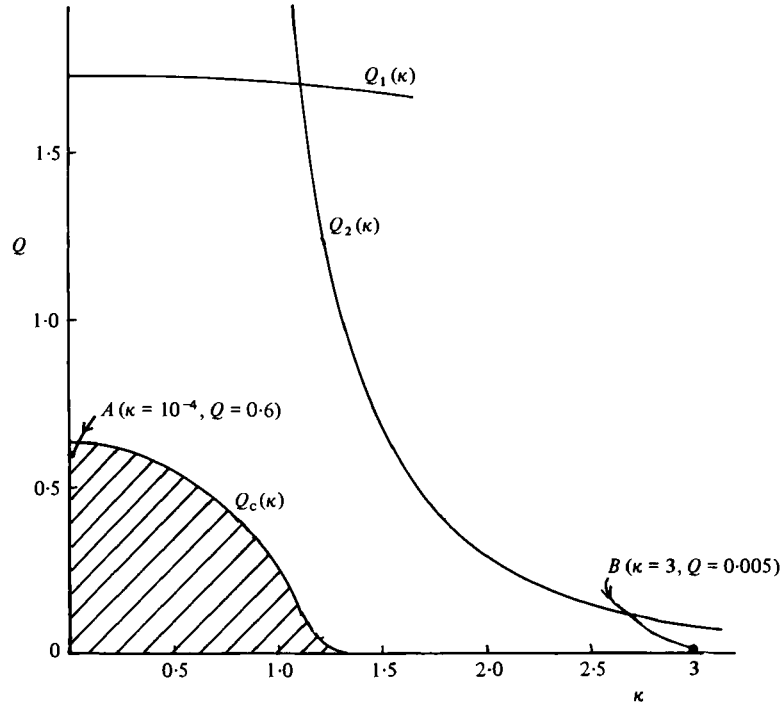

FIGURE 3. The hatched region, bounded by $Q = Q_c(\kappa)$, denotes the domain of the (κ, Q)-plane in which a steady inviscid solution exists. Runaway occurs if $Q > Q_c(\kappa)$. The necessary conditions for existence of a steady solution, obtained analytically, are $Q < Q_1(\kappa)$ and $Q < Q_2(\kappa)$. For profile evolution at the points A, B see figure 4.

$Q = Q_c(\kappa)$ is shown in figure 3, and it is evident that the necessary conditions (3.15) and (3.20) for the existence of a steady solution are by no means sufficient. The curve $Q = Q_c(\kappa)$ is characterized by a rapid fall-off for $\kappa \gtrsim 1$; the behaviour as $\kappa \to 0$ is quite regular, and $Q_c(0) = 0{\cdot}625$.

4. Effect of weak viscosity on the possible steady states

We return now to the steady form of (2.33a, b), viz

$$i\hat{U}f = (d^2/dy^2 - \kappa^2)f, \tag{4.1a}$$

$$(2Q)^{-1}\hat{U}|f|^2 = 1 + \epsilon\, d^2\hat{U}/dy^2. \tag{4.1b}$$

We shall suppose that $\epsilon \ll 1$; we then expect that, when Q is sufficiently small, the flow will be of Hartmann type (in the sense discussed in § 1), whereas, when Q is large, the field will be expelled, and the flow will be akin to Poiseuille flow. Let us first examine these limiting situations.

4.1. *Q small, Hartmann-type flow*

At leading order, the flow does not affect the magnetic field, and we have

$$f = \cosh\kappa\eta/\cosh\kappa, \tag{4.2}$$

and from (4.1b),

$$1 + \epsilon\frac{d^2\hat{U}}{d\eta^2} = \frac{1}{2Q}\hat{U}\frac{\cosh^2\kappa\eta}{\cosh^2\kappa}. \tag{4.3}$$

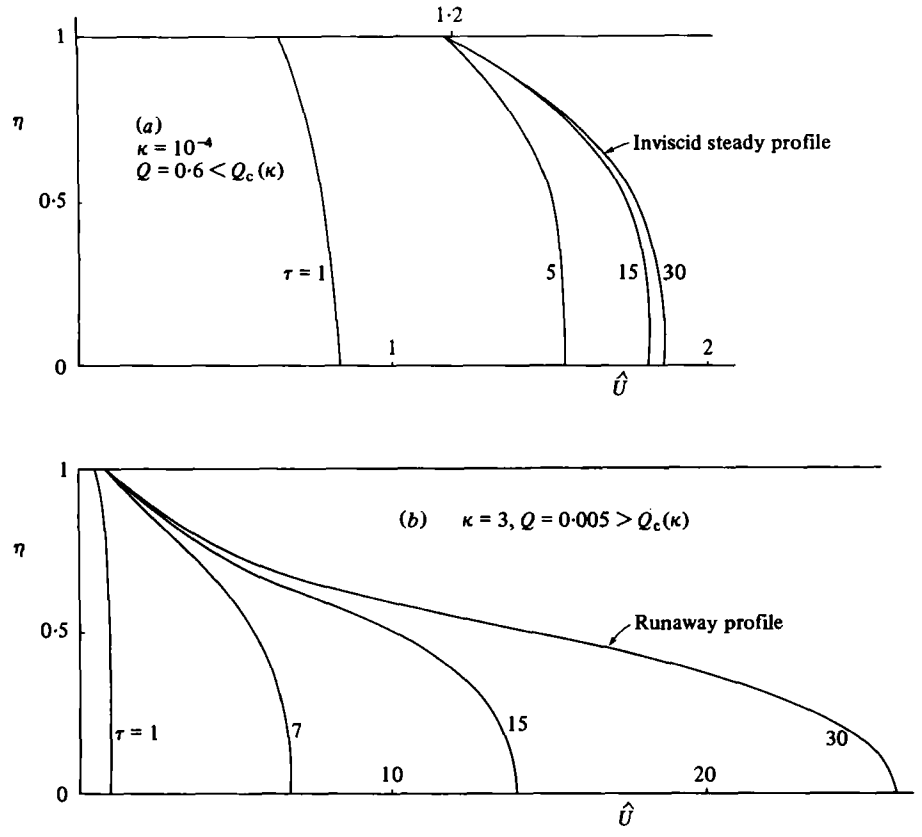

FIGURE 4. Typical evolution of velocity profiles: (*a*) when $Q < Q_c(\kappa)$; (*b*) when $Q > Q_c(\kappa)$. Note that in case (*a*), $\hat{U}(1) \to 2Q = 1{\cdot}2$ as $\tau \to \infty$, consistent with (3.4*c*). In case (*b*), the runaway effect is clear: the centreline velocity accelerates without limit.

With $\epsilon \ll 1$, we evidently have a Hartmann layer, thickness $\delta \sim \epsilon^{\frac{1}{2}}$ on both walls. In the core (i.e. outside these layers), the velocity is given by

$$\hat{U} \sim \hat{U}_c = 2Q \cosh^2 \kappa \operatorname{sech}^2 \kappa\eta. \tag{4.4}$$

In this region, there is an exact balance between pressure gradient and Lorentz force. The solution (4.4) does not, however, satisfy the no-slip condition on $\eta = \pm 1$; hence the need for the Hartmann layers, in which

$$\hat{U} \sim \hat{U}_H = 2Q\{1 - \exp(-(1-|\eta|)/(2\epsilon)^{\frac{1}{2}})\}, \tag{4.5}$$

satisfying

$$\lim_{\epsilon^{-\frac{1}{2}}(1-|\eta|)\to\infty} \hat{U}_H = \lim_{|\eta|\to 1} \hat{U}_c = 2Q. \tag{4.6}$$

The centreline velocity is given by

$$\hat{U}_0 = 2Q \cosh^2 \kappa. \tag{4.7}$$

The description is self-consistent if the term $i\hat{U}f$ in (4.1*a*) is negligible, i.e. if

$$Q \ll \kappa^2 \operatorname{sech}^2 \kappa. \tag{4.8}$$

For $\kappa \gtrsim 1$, this is a strong constraint, and if it is violated we may expect to be near, if not actually into, the runaway regime.

4.2. $Q \gg 1$, *Poiseuille-type flow*

In this situation, we expect the field to be expelled, so that $f \approx 0$ except in boundary layers on both walls. At leading order we then have

$$\epsilon d^2\hat{U}/d\eta^2 + 1 \approx 0, \tag{4.9}$$

so that

$$\hat{U} \approx (1-\eta^2)/2\epsilon, \tag{4.10}$$

i.e. the Poiseuille parabolic profile.

To improve on this description let

$$\hat{U} = (1-\eta^2)/2\epsilon + (\epsilon Q)^{-1}\hat{U}_1(\eta), \tag{4.11}$$

where $\hat{U}_1(\pm 1) = 0$. It will appear below that the $(\epsilon Q)^{-1}$ factor here correctly represents the order of magnitude of the small correction due to the Lorentz force in the boundary layer. At leading order, (4.1*a*) then becomes

$$(d^2/d\eta^2 - \kappa^2)f = -\tfrac{1}{2}i\epsilon^{-1}(\eta^2-1)f. \tag{4.12}$$

Here we shall suppose that κ is at most $O(1)$ and neglect the streamwise diffusion term $-\kappa^2 f$. Near $\eta = 1$, the appropriate boundary-layer variable is

$$\zeta = \epsilon^{-\frac{1}{3}}(1-\eta), \tag{4.13}$$

in terms of which (4.12) becomes

$$d^2f/d\zeta^2 \approx -i\zeta f, \tag{4.14}$$

and the solution, exponentially small for $\zeta \to \infty$, is

$$f(\zeta) = \alpha\,\mathrm{Ai}\,(e^{-\frac{1}{3}i\pi}\zeta) \tag{4.15}$$

where $\alpha\,\mathrm{Ai}\,(0) = 1$. Note that, as $\zeta \to \infty$,

$$f(\zeta) \sim \tfrac{1}{2}\alpha\pi^{-\frac{1}{2}}\zeta^{-\frac{1}{4}}\exp\left[-\tfrac{1}{24}i\pi - \tfrac{1}{3}\sqrt{2}\,\zeta^{\frac{3}{2}}(1-i)\right]. \tag{4.16}$$

Substitution of (4.11) and (4.15) in (4.1*b*) now gives, again using the boundary-layer variable ζ,

$$d^2\hat{U}_1/d\zeta^2 \approx \tfrac{1}{2}\alpha^2\zeta|\,\mathrm{Ai}\,(z)|^2 \quad (z = e^{-\frac{1}{3}i\pi}\zeta), \tag{4.17}$$

and the solution satisfying

$$\hat{U}_1 = 0 \quad \text{on} \quad \zeta = 0, \quad d\hat{U}_1/d\zeta \to 0 \quad \text{as} \quad \zeta \to \infty \tag{4.18}$$

is

$$\hat{U}_1(\zeta) = -\tfrac{1}{2}\alpha^2\left[\zeta\int_\zeta^\infty \zeta_1\,|\mathrm{Ai}\,(z_1)|^2 d\zeta_1 + \int_0^\zeta \zeta_1^2\,|\mathrm{Ai}\,(z_1)|^2 d\zeta_1\right]. \tag{4.19}$$

Note that, as $\zeta \to \infty$, $U_1(\zeta) \to -\hat{U}_s$, where

$$\hat{U}_s = \tfrac{1}{2}\alpha^2\int_0^\infty \zeta^2\,|\mathrm{Ai}\,(z)|^2 d\zeta. \tag{4.20}$$

The Poiseuille profile (4.10) is therefore retarded in the core by an amount $(\epsilon Q)^{-1}\hat{U}_s$; the effect of the magnetic field is simply to transmit this retardation through the boundary layers. The centreline velocity, from (4.11), is

$$\hat{U}(0) = (\tfrac{1}{2} - \hat{U}_s/Q)\,\epsilon^{-1}, \tag{4.21}$$

correct to order Q^{-1}.

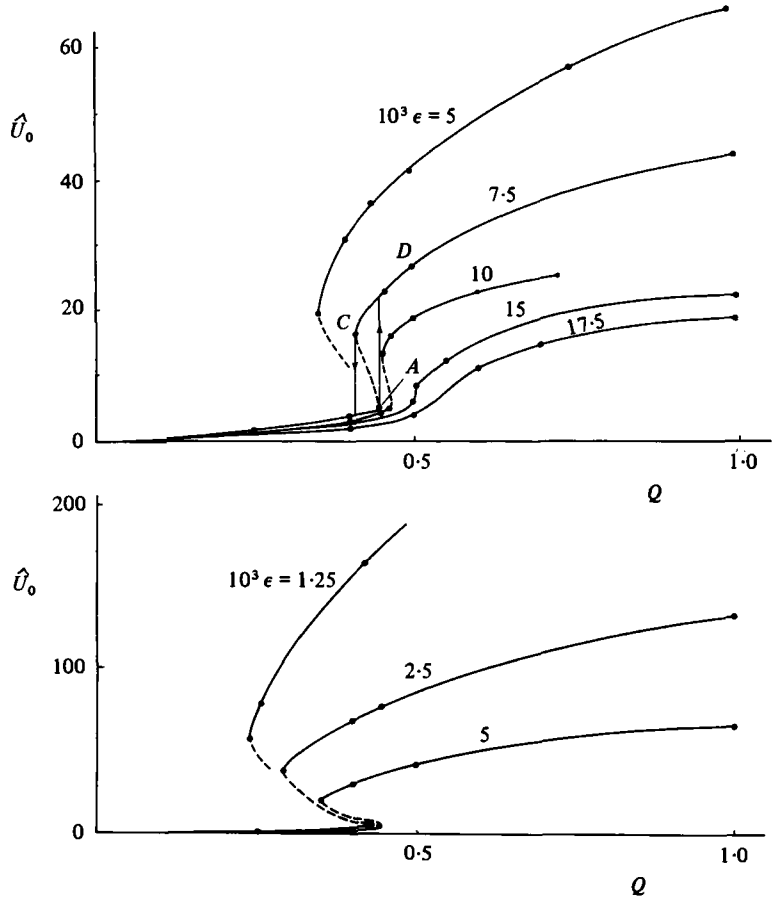

FIGURE 5. Centreline velocity U_0 as a function of Q for $\kappa = 1$ and various fixed values of ϵ. A fold appears for $\epsilon < 0{\cdot}015$. The dots represent computed steady states; the dashed portions represent unstable states. A jump from Hartmann-type flow to Poiseuille-type flow occurs at points such as A; a reverse jump occurs at points such as C.

5. Runaway and hysteresis effects when $\epsilon > 0$

We now turn to the evolution of the steady state as the parameter Q is increased through values of order unity. We may expect a jump from Hartmann-type flow to Poiseuille-type flow when Q is somewhat greater than the value $Q_c(\kappa)$ obtained in §3 on the basis of inviscid analysis (greater, because weak viscosity may be expected to have a mildly retarding effect on the velocity and so on the flux expulsion process).

Equations (2.33a, b) were integrated numerically for the case $\kappa = 1$, which is believed to be quite representative, for varying values of ϵ and Q. As indicated previously, the asymptotic steady-state behaviour does not depend on β, and the value $\beta = 1$ was used in the computations. It was found convenient to explore the (ϵ, Q)-plane by slowly increasing Q from small values, keeping ϵ constant. For the lowest value of Q, the initial conditions

$$f(\eta, 0) = \frac{\cosh \kappa\eta}{\cosh \kappa}, \quad \hat{U}(\eta, 0) = 0, \tag{5.1}$$

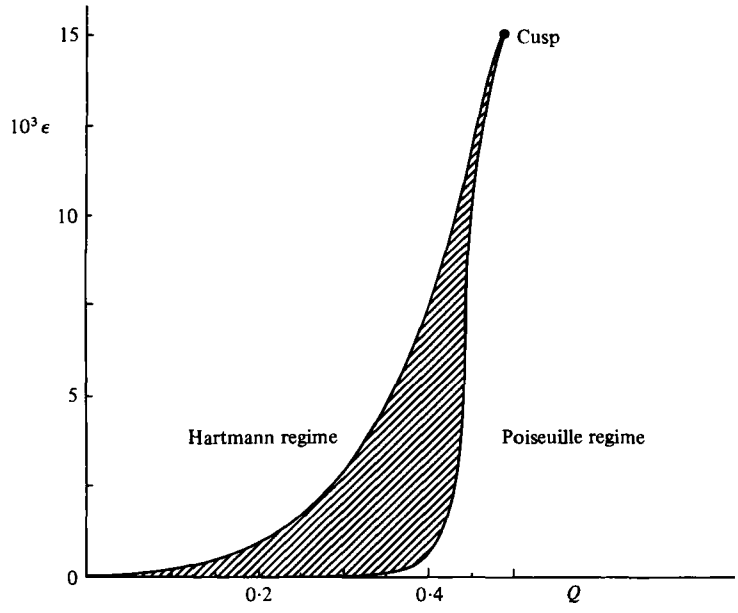

FIGURE 6. Projection on the (ϵ, Q)-plane of the fold in the surface $\hat{U}_0(\epsilon, Q)$, inferred from figure 5. In the shaded region of the parameter space, there are three steady solutions, one of Hartmann type, one of Poiseuille type, and one unstable.

were adopted, and the equations integrated until a steady state was attained, within acceptable accuracy. The corresponding values of f and $\hat{U}$ were then used as initial conditions for the next value of Q, and so on. The asymptotically steady centreline velocity $\hat{U}_0$ determined in this way is shown in figures 5(a, b) as a function of Q for various values of ϵ. As expected, the behaviour is discontinuous when ϵ is sufficiently small ($< 0{\cdot}015$ for $\kappa = 1$). The jump in $\hat{U}_0$ at a point such as A in figure 5(a) is just the runaway transition from a Hartmann-type flow to a Poiseuille-type flow in which the magnetic flux is effectively expelled. The value of Q at which this jump occurs depends on ϵ in the manner indicated in figure 6.

If we start with a Poiseuille-type profile at a point such as D in figure 5(a), and slowly *decrease* Q, then a reverse jump to a Hartmann-type profile occurs but is delayed to the point C, i.e. a hysteresis effect occurs. The value of Q corresponding to this reverse jump is also a function of ϵ, as shown in figure 6. Clearly, we are dealing here with a conventional cusp catastrophe, the shaded region in figure 6 representing values of Q and ϵ for which the solution is not unique (in fact, in this region, there are *three* solutions, but one of these, corresponding to the dashed portions of the curves in figures 5(a, b), is structurally unstable). Regarding the centreline velocity $\hat{U}_0$ as a (triply-valued) function of ϵ and Q, the cusp-shaped region in figure 6 is the projection of the fold in the surface $\hat{U}_0 = \hat{U}_0(\epsilon, Q)$.

6. Discussion

The detailed calculations of §§2–5 are entirely consistent with the qualitative description of the runaway phenomenon given in §1, and provide convincing evidence that this description is essentially correct. The phenomenon occurs essentially because

$\langle B_y \rangle = 0$ on $y = 0$, so that flux expulsion can occur through reconnection of flux lines as Q increases. The particular sinusoidal distribution of B_y assumed in (1.1) is mathematically convenient, but any periodic distribution of B_y with zero mean in the x-direction would presumably lead to similar behaviour.

Throughout the analysis we have assumed that the flow is laminar, which is not unreasonable in the Hartmann regime of figure 6 in which the magnetic field will tend to stabilize disturbances in the strong shear regions near the walls (Lock 1955). When Q is increased beyond the critical value $Q_c(\kappa)$, however, the Reynolds number of the flow (based on mean velocity) increases by a factor of order $(Q\epsilon)^{-1}$ (from comparison of (4.4) and (4.10)), which may obviously lead to a turbulent state. The developing profiles of figure 4(*b*) show points of inflexion, which again suggests that instabilities may be expected as we move into the runaway regime. Consequently, the runaway phenomenon may in practice be observed as a sudden increase of flow rate (for infinitesimal increase of pressure gradient) with a simultaneous transition to turbulence.

Let us now consider the possibility of an experiment to detect the runaway effect. The most convenient fluid would (presumably) be mercury for which $P_m \approx 1{\cdot}7 \times 10^{-7}$. If we take $\kappa = 1$, then it is evident from figure 5 that, to detect the runaway effect, we should vary Q between about 0·25 and 1, with $\epsilon < 0{\cdot}015$. If we take $\epsilon = 0{\cdot}01$ then, from (2.36), $\beta \approx 1{\cdot}7 \times 10^{-5}$ and the inequality (2.35) is easily satisfied. Moreover

$$M = (Q\epsilon)^{-\frac{1}{2}} = 10Q^{-\frac{1}{2}}, \tag{6.1}$$

so that we are dealing with a very modest range of Hartmann numbers. The corresponding centreline velocity $\hat{U}_0$ jumps from about 4 to about 15 when the runaway occurs (for this value of ϵ). From (2.32), this means that the magnetic Reynolds number based on the (dimensional) centreline velocity U_0, viz

$$R_m = U_0 b/\lambda = \hat{U}_0 \kappa^{-1}, \tag{6.2}$$

has a similar jump at runaway. Herein lies the main difficulty of an experiment, since values of the magnetic Reynolds number of order unity are difficult to achieve in mercury experiments. Increasing the value of κ will decrease the value of $Q_c(\kappa)$, but this is compensated by an associated increase in the centreline velocity U_0 given by (4.7), and the magnetic Reynolds number at the runaway point remains of order unity (or greater).

A possible way round this difficulty would be to use a *travelling* magnetic field, with phase velocity $-c$ at both walls; the effective magnetic Reynolds number for flux expulsion purposes is then

$$R_m^{(\text{eff})} = (U_0 + c)\, b/\lambda, \tag{6.3}$$

and cb/λ can be chosen near to the critical value so that a relatively small increase $U_0 b/\lambda$ will trigger the runaway effect. The boundary conditions are of course changed by this artifice, and an additional parameter cb/λ appears in the specification of the problem. This extension would however appear to merit further study. There is no doubt that a travelling field can be used to simulate high-magnetic-Reynolds-number effects, and this provides additional scope in the use of magnetic fields for flow control.

Two final remarks: first, if the condition (2.26) is not satisfied, i.e. if $B_0^4 \gtrsim k(\mu_0 \rho \lambda)^2 G$, then the magnetic field is so strong that the fluid particles tend to follow the field lines except in wall boundary layers; consequently the fluctuation field $\mathbf{u}'$ becomes comparable with the mean $U\mathbf{i}_x$. This is similar to the strong-field limit studied in the rotating-field context by Alemany & Moreau (1977).

Secondly, as noted earlier, the runaway phenomenon occurs essentially because $\langle B_y \rangle = 0$ on $y = 0$. The situation is however entirely different if the applied field is such that B_y is zero for all x on $y = 0$. For example, if the magnets of figure 1 are shifted in phase so that the boundary condition (1.1) is replaced by

$$B_y = \pm B_0 \cos kx \quad \text{on} \quad y = \pm b, \tag{6.3}$$

then $B_y \equiv 0$ on $y = 0$ by symmetry. In this case there is no steady inviscid solution for any value of G (no matter how small); in a sense therefore the runaway effect now occurs at $G = 0$! When $\epsilon > 0$, however, there is no reason to expect discontinuous dependence of U on Q in this case, which is therefore qualitatively different from that studied in the foregoing sections.

REFERENCES

ALEMANY, A. & MOREAU, R. 1977 Écoulement d'un fluide conducteur de l'électricité en présence d'un champ magnétique tournant. *J. Méc.* **16**, 625–646.

GALLOWAY, D. J., PROCTOR, M. R. E. & WEISS, N. O. 1978 Magnetic flux ropes and convection. *J. Fluid Mech.* **87**, 243–261.

GIMBLETT, C. G. & PECKOVER, R. S. 1979 On the mutual interaction between rotation and magnetic fields for axisymmetric bodies. *Proc. R. Soc. Lond.* A **368**, 75–97.

HUNT, J. C. R. & SHERCLIFF, J. A. 1971 Magnetohydrodynamics at high Hartmann number. *Ann. Rev. Fluid Mech.* **3**, 37.

KAMKAR, H. 1981 Kinematic and dynamic aspects of flux expulsion in magnetohydrodynamics. Ph.D. thesis, Bristol University.

LOCK, R. C. 1955 The stability of the flow of an electrically conducting fluid between parallel planes under a transverse magnetic field. *Proc. R. Soc. Lond.* A **233**, 105–125.

MOFFATT, H. K. 1980 Rotation of a liquid metal under the action of a rotating magnetic field. In *MHD-Flows and Turbulence* (ed. H. Branover & A. Yakhot), pp. 45–62. Israel Universities Press.

PARKER, E. N. 1963 Kinematical hydromagnetic theory and its applications to the low solar photosphere. *Astrophys. J.* **138**, 552–575.

PARKER, R. L. 1966 Reconnexion of lines of force in rotating spheres and cylinders. *Proc. R. Soc. Lond.* A **291**, 60–72.

PROCTOR, M. R. E. & GALLOWAY, D. J. 1979 The dynamic effect of flux ropes on Rayleigh–Bénard convection. *J. Fluid Mech.* **90**, 273–287.

WEISS, N. O. 1966 The expulsion of magnetic flux by eddies. *Proc. R. Soc. Lond.* A **293**, 310–328.

ZEL'DOVICH, YA. B. 1957 The magnetic field in the two-dimensional motion of a conducting turbulent fluid. *Sov. Phys. J.E.T.P.* **4**, 460–462.